JOURNAL OF SOLID STATE CHEMISTRY 38, 335–341 (1981)

The Electrical Conductivity and Thermoelectric Power of Mn_3O_4 at High Temperatures

R. METSELAAR, R. E. J. VAN TOL, AND P. PIERCY

Laboratory of Physical Chemistry, Eindhoven University of Technology, Eindhoven, The Netherlands

Received September 6, 1980; in final form December 29, 1980

The electrical resistivity and the Seebeck coefficients of Mn_3O_4, in the temperature range 1100–1700 K, have been measured under oxygen partial pressures of $1–10^{-6}$ atm. The resistivity is thermally activated with an activation energy of 1.3 eV for the tetragonal (low-temperature) phase and 0.65 eV for the cubic (high-temperature) phase. The thermoelectric power shows p-type behavior with an activation energy of 1.1 eV for the tetragonal phase and 0.3 eV for the cubic phase. The data can be explained satisfactorily in terms of small-polaron hopping.

1. Introduction

Though there exists extensive literature on electrical transport properties of transition metal oxides, relatively little is known about Mn_3O_4. Also, among the various types of manganese oxides, Mn_3O_4 has drawn the least attention as far as transport properties are concerned. The purpose of our present investigation is to obtain more insight into these properties.

In nature Mn_3O_4 occurs as the mineral hausmannite. This is a tetragonally deformed spinel, space group D_{4h}^{19}, with $c/a = 1.16$ (*1*). Above a critical temperature T_t the hausmannite, or α phase, undergoes a first-order phase transition to the β phase with cubic spinel structure. From high-temperature X-ray diffractometry it is deduced that $T_t = 1433$ K (*2*). As indicated in Fig. 1, the Mn_3O_4 phase is stable in air only in the range 1153–1840 K (*3*). According to Schmahl and Hennings (*4*) the temperature of 1840 K is the eutectic temperature of the system Mn_3O_4–MnO. Below 1153 K, Mn_3O_4 transforms to Mn_2O_3. At low P_{O_2}, Mn_3O_4 transforms to MnO as shown in Fig. 1. The equilibrium data for the phase boundaries Mn_3O_4–MnO and Mn_3O_4–Mn_2O_3 have been reported by several investigators (*3–5*).

Measurements of the electrical resistivity have been reported by Romeijn (*6*) and by Logothetis and Park (*7*). Romeijn found a discontinuity in the resistivity in the temperature region 1350–1425 K, with a marked thermal hysteresis. According to this author the resistivity is an exponential function of temperature with an activation energy of 1.3 eV for the tetragonal phase and 0.75 for the cubic phase. The value of 1.3 eV for the α phase has been confirmed by Ref. (*7*). As pointed out by the last-mentioned authors, values of 0.75 (*8*) and 0.65 eV (*9*), obtained from resistivity measurements in the temperature range 0–400°C should be discarded. The reason is that these measurements were performed on samples which were quenched from a high temperature and therefore probably

0022-4596/81/090335-07$02.00/0

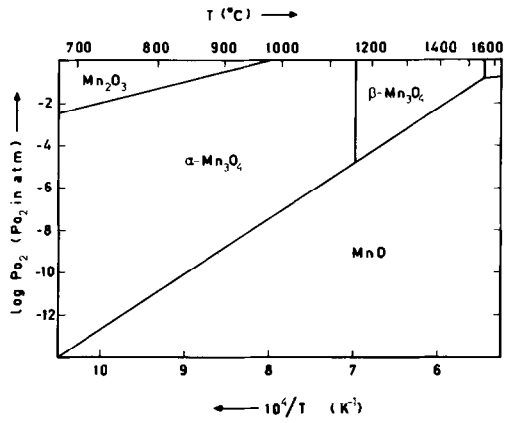

FIG. 1. Part of the phase equilibrium diagram for the system Mn–O.

contaminated with a surface layer of Mn_2O_3.

The cation valencies in Mn_3O_4 have been the subject of several discussions. Some authors assume the formula $Mn^{2+}[Mn^{2+}Mn^{4+}]O_4$, where the ions between square brackets are on the octahedral sites of the spinel lattice (*10, 11*). However, much more evidence has been presented in favor of the formula $Mn^{2+}[Mn_2^{3+}]O_4$; evidence which was mainly based on measurements of resistivity in solid solutions of manganese spinels (*12*), X-ray diffraction (*13, 14*) and magnetic properties (*15*). As a result of a comparison between experimental data and theoretical considerations Goodenough and Loeb (*16*) also concluded in favor of the latter formula.

In this paper we will discuss measurements of the electrical resistivity and thermoelectric power of Mn_3O_4 in the temperature range 1100–1700 K, at different oxygen partial pressures. In Section 2 the experimental method will be discussed; in Section 3 the results of measurements of the electrical resistivity and the thermoelectric power of Mn_3O_4 will be presented. Subsequently an analysis of these results will be given in Section 4.

2. Experimental Method

Manganese oxide was obtained by decomposition of high-purity $MnCO_3 \cdot x$ aq. (Merck). After quenching to room temperature the powder was ball-milled. Pellets were sintered at 1620 K for 16 hr. The density of the samples was 97%, with a grain size of 14 μm (mean intercept length). Spectrochemical analysis of the sintered samples showed the following impurity levels (in weight ppm): 50 Mg, 8 Cu, 50 Fe, 80 Al, 50–100 Si. The electrical measurements were performed on sintered samples with dimensions 8 × 4 × 1 mm. To obtain samples with higher purity, sintered bars were zone melted with the aid of an arc-image furnace (*17*). In an attempt to produce single crystals from the sintered bar a ⟨110⟩ seed crystal was used. Due to the transition from the high-temperature cubic phase to the tetragonal phase, however, multiply twinned crystals were obtained. The impurity levels (in weight ppm) were: 7 Mg, 4 Cu, 40 Fe, 4 Si. Electrical measurements were performed on crystals with a length of 7 mm and a diameter of 5 mm ø. Four-probe techniques were employed to measure the dc conductance; a strictly ohmic behavior was observed. It was verified that ac measurements gave identical results. Pt voltage and current leads were fixed to the sample with the aid of platinum paste (Emetron). Pt 10% Rh–Pt thermocouples were used both for measurements of the sample temperature and of the thermoelectric power. For the latter purpose a gradient up to 20 K could be applied over the length of the sample. At a given sample temperature the thermoelectric voltage ΔV was measured as a function of ΔT and the Seebeck coefficient was obtained from the slope of the ΔV versus ΔT plot. The values were corrected for the absolute thermopower of platinum (*18*). After prolonged heating, e.g., 4 weeks at 1620 K, islands of about 40 μm of Pt were

observed in the region adjacent to the contacts. No influence on the conductance could be observed, however. The partial oxygen pressure around the sample was varied between 1 and 10^{-6} atm using O_2–Ar mixtures with a controlled flow. The partial oxygen pressure was measured both at the inlet and outlet of the measuring cell with the aid of stabilized zirconia oxygen gauges. Details of the measuring cell have been published earlier (*19*).

3. Experimental Results

For a number of both sintered and melt-grown samples the resistance and Seebeck coefficients were measured over a range of temperatures. Figure 2 gives an example for a sintered sample at $P_{O_2} = 1$ atm. Figure 2a shows a straight line for $\ln \rho$ vs T^{-1}. The activation energy for the tetragonal (α) phase is about 1.35 eV. At about 1430 K a drop in the resistivity is observed due to the transition to the cubic (β) phase. A hysteresis of about 25 K is observed. The activation energy of the β phase is about 0.65 eV. The arrow at $T = 1250$ K indicates the limit of the stability region of Mn_3O_4 at 1 atm. As has been observed earlier (*7*) the phase transition $Mn_3O_4 \rightarrow Mn_2O_3$ is very slow in this temperature region and no discontinuity in the resistance is observed even after 2 hr. Data in the form of the reduced Seebeck coefficient $\alpha e/k$ are shown in Fig. 2b as a function of temperature. In all cases studied here, only p-type behavior has been found. The activation energy calculated from this plot is about 1.2 eV for the α phase and 0.3 eV for the β phase.

The difference in activation energies between the resistivity and the Seebeck coefficients suggests that the charge transport is due to a thermally activated process, as has been observed for most compounds with the spinel structure. For this reason we have plotted $\ln(\rho/T)$ vs T^{-1} in Figs. 3–5. The corresponding data for the Seebeck coefficient $\alpha e/k$ are displayed on the same scale in these figures. Within the experimental accuracy both plots of $\ln \rho$ and of $\ln(\rho/T)$ vs T^{-1} yield linear relationships for this small temperature region. Figure 3 shows the $\ln(\rho/T)$ data for a sintered

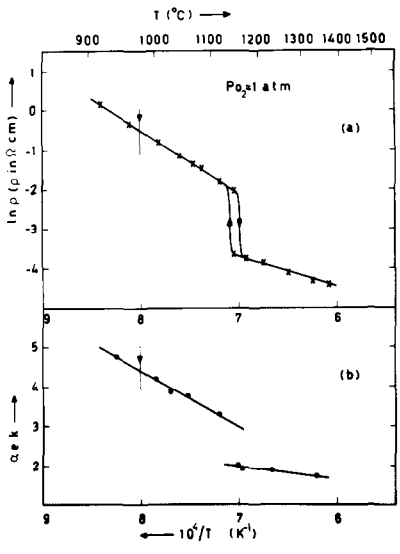

FIG. 2. Temperature dependence of the resistivity (a) and reduced Seebeck coefficient (b) for a sintered sample of Mn_3O_4 at 1 atm oxygen partial pressure. At temperatures above 1250 K, indicated by the arrow, Mn_3O_4 is metastable.

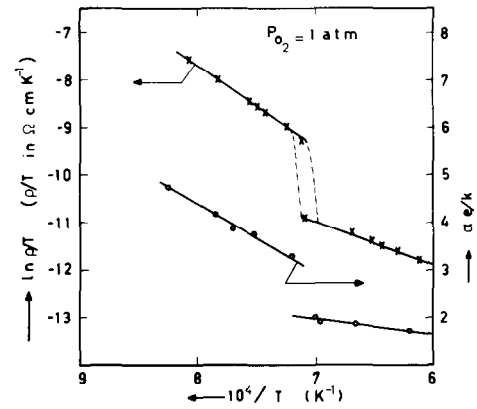

FIG. 3. Combined plot of resistivity, $\ln(\rho/T)$, and reduced Seebeck coefficient $\alpha e/k$ vs reciprocal temperature, for a sintered sample of Mn_3O_4 at 1 atm oxygen partial pressure.

sample at $P_{O_2} = 1$ atm. Lower oxygen pressures were used to enable measurements of the α phase over a larger temperature range. Figure 4 shows data for a melt-grown sample at $P_{O_2} = 2.5 \times 10^{-4}$ atm, while Fig. 5 shows the results obtained for a sintered sample under the same conditions. Figure 6 shows the dependence of the resistivity at a given temperature as a function of the oxygen partial pressure. The arrows indicate the phase boundary Mn_3O_4–MnO at each temperature. It can be seen that the pressure dependence of the resistivity is weak, except close to the phase boundary where the resistivity increases more strongly.

Table I summarizes relevant data from Figs. 2–6. Both the activation energies and the intercepts at $T^{-1} = 0$ of the plots of ln (ρ/T) and $\alpha e/k$ vs T^{-1} are given.

4. Discussion

All samples show extrinsic, p-type behavior. In this case we have

$$\ln \rho = -\ln pe\mu, \qquad (1)$$

where p is the concentration of positive charge carriers, e is the absolute value of the electronic charge, and μ is the drift mobility.

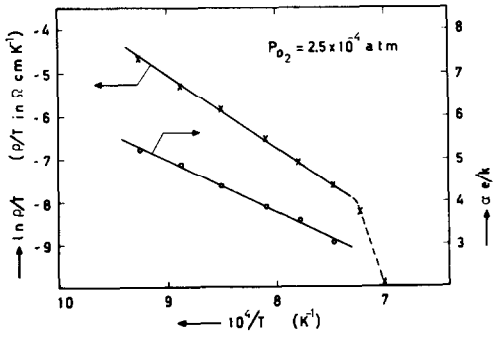

FIG. 4. Combined plot of the resistivity and reduced Seebeck coefficient vs reciprocal temperature, for a melt-grown sample of Mn_3O_4 at an oxygen partial pressure of 2.5×10^{-4} atm.

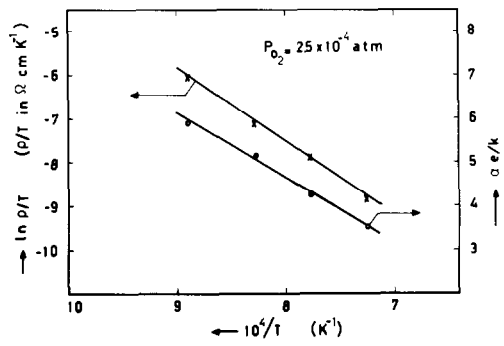

FIG. 5. Combined plot of the resistivity and reduced Seebeck coefficient vs reciprocal temperature, for a sintered sample of Mn_3O_4 at an oxygen partial pressure of 2.5×10^{-4} atm.

The Seebeck coefficient α can be expressed as:

$$\alpha = k/e\,[A + \ln(N_v/p)], \qquad (2)$$

where N_v is the effective density of states in the valence band and A is a constant depending on the dominant scattering mechanism. The ratio N_v/p is determined by the position of the Fermi level (E_F) with respect to the top of the valence band:

$$p = N_v \exp(-E_F/kT). \qquad (3)$$

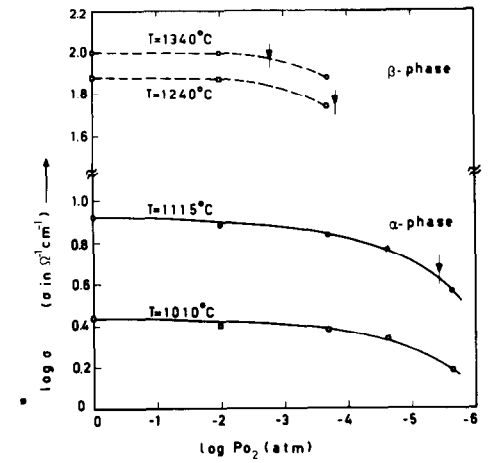

FIG. 6. Oxygen pressure dependence of the resistivity of a sintered sample of Mn_3O_4 at different temperatures. The vertical arrows designate the phase boundary Mn_3O_4–MnO; on the low-pressure side Mn_3O_4 is metastable.

TABLE I

ACTIVATION ENERGIES DETERMINED FROM THE SLOPES OF ln ρ, ln(ρ/T), AND $\alpha e/k$ VS T^{-1}; EXTRAPOLATED VALUES ln(ρ_0/T) AND $\alpha_0 e/k$ AT $T^{-1} = 0$ K^{-1}[a]

Sample	Activation energies in eV			Intercepts at $T^{-1} = 0$	
	$E(\rho)$	$E(\rho/T)$	$E(\alpha e/k)$	$\ln(\rho_0/T)$	$\alpha_0 e/k$
α phase					
Melt-grown	1.30	1.42	1.04	−20.3	−5.8
Sintered	1.34	1.45	1.17	−21.1	−7.1
Ref. (6)	1.3	—	—	−20.7	
β phase					
Sintered	0.65	0.78	0.26	−17.2	−0.4
Ref. (6)	0.67	—		−16.3	

[a] The estimated uncertainties in $E(\rho)$ and $E(\rho/T)$ are ±0.05 eV; in $E(\alpha e/k)$ ±0.1 eV; in $\ln(\rho_0/T)$ ±0.5; in $\alpha_0 e/k$ ±1.0.

For a small-polaron semiconductor the mobility can be written as

$$\mu = \frac{ed^2\nu_0}{kT} \exp\left(\frac{-E_\mu}{kT}\right), \quad (4)$$

where d is the jump distance and ν_0 is the optical phonon frequency. From these equations it follows that

$$\ln(\rho/T) = -\ln(N_v e^2 d^2 \nu_0/k) + (E_F + E_\mu)/kT, \quad (5)$$

$$\alpha e/k = A + (E_F/kT). \quad (6)$$

The activation energy of the mobility (E_μ) as determined from the slopes of the ln(ρ/T) and $\alpha e/k$ vs T^{-1} plots are given in Table II. Due to the limited temperature range the accuracy in the activation energy is only about 0.05 eV for the resitivity curves and about 0.1 eV for the plots of the Seebeck coefficients. From Table II it is seen that $E_\mu \sim 0.33$ eV for the tetragonal phase and 0.5 eV for the cubic phase. The position of the Fermi level of this partially compensated semiconductor is approximated by:

$$E_F = E_A + kT \ln[gN_D/(N_A - N_D)], \quad (7)$$

where E_A is the position of the acceptor level with respect to the top of the valence band, N_D is the donor concentration, N_A the acceptor concentration, and g a degeneracy factor (*20*).

The constant A is connected with the kinetic electron energy. If the conduction takes place via a broad band, the value of A

TABLE II

SOME CONSTANTS DERIVED FROM THE DATA IN TABLE I UNDER THE ASSUMPTION OF SMALL-POLARON HOPPING OVER OCTAHEDRAL SITES[a]

Sample	E_μ (eV)	E_A (eV)	C	ν_0 (10^{13} sec^{-1})	μ at 1200 K (cm^2 V^{-1} sec^{-1})
α phase					
Melt-grown	0.38	1.04	350	2.4	5.3×10^{-3}
Sintered	0.28	1.17	1200	1.4	8.1×10^{-3}
β phase	0.52	0.26	2	23	1.3×10^{-2}

[a] See text.

equals about 2. For a small-polaron semiconductor the precise value of A is less certain. It is generally assumed that in the latter case A is zero or close to zero (*20*).

Assuming $A = 0$, Eqs. (5) and (6) can be written as

$$\ln(\rho/T) = \ln(k/N_v e^2 d^2 \nu_0) - \ln C + (E_A + E_\mu)/kT, \quad (8)$$

$$\alpha e/k = -\ln C + (E_A/kT), \quad (9)$$

where

$$C = (N_A - N_D)/gN_D.$$

This means that the activation energy of the Seebeck coefficient is equal to E_A.

The intercept of the $\alpha e/k$ vs T^{-1} plot at $T^{-1} = 0\ K^{-1}$ gives the compensation degree C. The resulting data are shown in Table II. Since we have to extrapolate over a large temperature range, the values have a high uncertainty, e.g., in the worst case we estimate that the value of C given in the first line lies between 120 and 900, in the second line between 450 and 3000. However, the ratio N_A/N_D is clearly larger for the sintered sample. Since the impurity content does not change at the phase transition, the change of C from 1200 in the tetragonal phase to 2 in the cubic phase, is unexpectedly large. This is due either to the uncertainty of the extrapolation, or to a change in the concentration of native defects at the transition temperature.

As has been indicated in the introduction, it is generally assumed that Mn_3O_4 should be written as $Mn^{2+}[Mn_2^{3+}]O_4$. Values of N_v and d may then be estimated on the supposition that the hopping process involves electron exchange between Mn ions on adjacent octahedral sites in the spinel lattice. With a lattice parameter $a = 8.6$ Å, we find $d = \frac{1}{4}a2^{1/2} = 3.0$ Å. For a small-polaron semiconductor the density of states, N_v, equals twice the concentration of cations available as a site for the small polaron. This gives $N_v = 32/a^3 = 5 \times 10^{22}$ cm^{-3}. With the aid of these data we obtain the jump frequency ν_0 as shown in Table II. For the α phase we find $\nu_0 \approx 2 \times 10^{13}$ sec^{-1}, which is in the frequency range expected for optical phonons. The value of ν_0 for the β phase is evidently too high. Table II also shows the mobility values calculated for $T = 1200$ K; for the α phase $\mu \approx 0.006$ $cm^2/V \cdot sec$. In view of the uncertainty in the data, especially for the β phase, it should not be concluded that the mobility in the β phase extrapolated to 1200 K is a factor of 2 higher than in the α phase.

Let us next consider the changes at the phase transition. At the transition temperature the two phases are in equilibrium with each other; i.e., the Fermi level lies at the same energy. From the measured Seebeck coefficient we calculate $E_F(T) = e\alpha T$. At the phase transition temperature $T_t = 1428$ K ($T_t^{-1} = 7 \times 10^{-4}$ K^{-1}) we find $e\alpha T_t = 0.37$ eV for the α phase and 0.24 eV for the β phase. This means that the phase transition is accompanied by a shift of 0.13 eV of the top of the valence band with respect to the Fermi level.

Finally, a few words should be said about the role of the impurities. The foreign ions found to be present are Cu, Mg, Fe, Al, and Si. From the literature on manganates we conclude that iron and aluminum are present as trivalent ions on octahedral sites (*21*). As such these ions will scarcely influence the resistivity. Silicon is tetravalent and will be a donor irrespective of the site. Copper can be present as Cu^+ on tetrahedral sites (*21*) or as Cu^{2+} on octahedral sites (*12*). In both cases it will act as acceptor. According to Driessens (*21*) magnesium is mainly on tetrahedral sites at low temperatures. However, above 1100 K the amount of Mg^{2+} on octahedral sites increases very rapidly. Such a change in the degree of inversion results in a change in the acceptor concentration.

In the melt-grown sample we find 1.0×10^{18} cm^{-3} for the sum of the copper and magnesium concentrations, and

0.4×10^{18} cm^{-3} for silicon. In the sintered samples [Mg] + [Cu] = 6.4×10^{18} cm^{-3}, while the silicon concentration in different samples varied between 5 and 10×10^{18} cm^{-3}. No doubt the silicon has been introduced during the milling process with agate balls. It is not certain that all of the silicon is dissolved in the Mn_3O_4 because one sample which contained 7×10^{19} cm^{-3} of silicon was still found to be p-type.

Literature data on native defects in Mn_3O_4 are scarce. Hahn and Muan (*1*) report very small deviations from stoichiometry. Le Blanc and Wehner (*22*) give an upper limit of 1.42 for the O/Mn ratio, while Schmier and Sterr (*23*) give 1.40 at 670 K. Since Mn_3O_4 consists essentially of an fcc oxygen lattice, the defects are probably manganese vacancies. Schmahl and Hennings (*4*) have investigated the compositions at the phase boundary with MnO. Above 1570 K, i.e., in the β- Mn_3O_4 phase, the solubility of MnO in Mn_3O_4 increases with increasing temperature. The ratio O/Mn decreases from 1.32 at 1655 K to 1.30 at 1700 K and 1.26 at 1800 K under the equilibrium oxygen pressure (cf. Fig. 1). Our own measurements indicate that the degree of compensation changes when going from the tetragonal to the cubic phase. This is confirmed by Romeijn's data (*6*): his extrapolated ln ρ_0 values indicate an increase in ρ_0 by a factor of 80, while our data result in a factor of 50. Since the concentration of foreign ions does not change, we conclude that the number of native point defects does change indeed at the phase transition.

Apart from the change due to a structural transformation, there is also a change as a function of temperature and oxygen partial pressure. As shown in Fig. 6 the resistivity at constant temperature is nearly constant in the region $P_{O_2} = 1$ atm up to the limit of the stability region of Mn_3O_4 (indicated by arrows in Fig. 6). From this we deduce that the resistivity is dominated by impurity ions.

Acknowledgments

Thanks are due to V. A. M. Brabers for supplying the melt-grown samples and to G. Oversluizen for discussions about the subject matter of this paper.

References

1. D. R. Petzold, *Krist. Tech.* **6,** 53 (1971).
2. H. J. van Hook and M. L. Keith, *Amer. Mineral.* **43,** 69 (1958).
3. W. C. Hahn, Jr. and A. Muan, *Amer. J. Sci.* **258,** 66 (1960).
4. M. G. Schmahl and D. F. K. Hennings, *Arch. Eisenhüttenw.* **40,** 395 (1969).
5. F. Shenouda and S. Ariz, *J. Appl. Chem.* **17,** 258 (1967).
6. F. C. Romeyn, *Philips Res. Rep.* **8,** 304 (1953).
7. E. M. Logothetis and K. Park, *Solid State Commun.* **16,** 909 (1975).
8. E. G. Larson and R. J. Arnott, *J. Phys. Chem. Solids* **23,** 1771 (1962).
9. J. P. Suchet, "Crystal Chemistry and Semiconduction in Transition Metal Binary Compounds," p. 183. Academic Press, New York (1971).
10. M. E. Fine and C. Chiou, *Phys. Rev.* **105,** 121 (1957).
11. S. M. Ariya and N. M. Enden, *J. Struct. Chem. USSR* **11,** 570 (1970).
12. M. Rosenberg, P. Nicolau, R. Manaila, and P. Pausescu, *J. Phys. Chem. Solids* **24,** 1419 (1963).
13. M. Nogúes and P. Poix, *J. Solid State Chem.* **9,** 330 (1974).
14. G. I. Finch, A. P. B. Sinha, and K. P. Sinha, *Proc. Roy. Soc. A* **242,** 28 (1957).
15. B. Boucher, R. Buhl, and M. Perrin, *J. Phys. Chem. Solids* **32,** 2429 (1971).
16. J. B. Goodenough and A. L. Loeb, *Phys. Rev.* **98,** 391 (1955).
17. V. A. M. Brabers, Thesis, Eindhoven University of Technology (1970).
18. N. Cusack and P. Kendall, *Proc. Phys. Soc. London* **72,** 898 (1958).
19. P. K. Larsen and R. Metselaar, *Phys. Rev.* **14,** 2520 (1976).
20. A. J. Bosman and H. J. van Daal, *Adv. in Phys.* **19,** 1 (1970).
21. F. C. M. Driessens, *Inorg. Chim. Acta* **1,** 193 (1967).
22. M. Le Blanc and G. Wehner, *Z. Phys. Chem. A* **168,** 59 (1934).
23. A. Schmier and G. Sterr, *Z. Anorg. Allg. Chem.* **346,** 181 (1966).